

Measurement of the Higgs Boson Mass with a Linear e^+e^- Collider

P. Garcia-Abia,
CIEMAT, Madrid

W. Lohmann and A. Raspereza
DESY

March 22, 2018

Abstract

The potential of a linear e^+e^- collider operated at a centre-of-mass energy of 350 GeV is studied for the measurement of the Higgs boson mass. An integrated luminosity of 500 fb^{-1} is assumed. For Higgs boson masses of 120, 150 and 180 GeV the uncertainty on the Higgs boson mass measurement is estimated to be 40, 65 and 70 MeV, respectively. The effects of beam related systematics, namely a bias in the beam energy measurement, the beam energy spread and the luminosity spectrum due to beamstrahlung, on the precision of the Higgs boson mass measurement are investigated. In order to keep the systematic uncertainty on the Higgs boson mass well below the level of the statistical error, the beam energy measurement must be controlled with a relative precision better than 10^{-4} .

1 Introduction

In the Standard Model [1] particles acquire mass due to spontaneous symmetry breaking by introducing a doublet of complex scalar fields. This so called Higgs mechanism [2] leads to one scalar particle, the Higgs boson. The mass of the Higgs boson is a free parameter of the Standard Model and of fundamental nature. If the Higgs boson exists, the Large Hadron Collider at CERN will be able to discover it [3]. Precision measurements of the Higgs boson parameters and the exploration of the complete Higgs boson profile will be one of the central tasks at a future linear e^+e^- collider.

In this article we study the potential of a future e^+e^- collider for the measurement of the mass of a relatively light Higgs boson, in the mass

range from 120 to 180 GeV, and investigate possible systematic effects influencing the precision of this measurement. The analysis presented extends previous studies on the measurement of the mass of a light Higgs boson [4] and complements recent studies on the determination of resonance parameters of the Higgs boson with the mass in the range from 200 to 320 GeV at a future linear e^+e^- collider [5].

2 Experimental Conditions and Detector Simulations

The study is performed for a linear collider operated at a centre-of-mass energy, \sqrt{s} , of 350 GeV and an event sample corresponding to an integrated luminosity of 500 fb^{-1} . This integrated luminosity is expected in about one year of running with design luminosity.

The detector used in the simulation follows the proposal for the TESLA collider presented in the Technical Design Report [6]. The interaction region is surrounded by a central tracker consisting of a silicon micro-vertex detector as the innermost part and a time projection chamber. In radial direction follow an electromagnetic calorimeter, a hadron calorimeter, the coils of a superconducting magnet and an instrumented iron flux return yoke. The solenoidal magnetic field is 4T. The central tracker momentum resolution is

$$\frac{\sigma_{p_t}}{p_t} = 7 \cdot 10^{-5} \cdot p_t, \quad (1)$$

where p_t is the transverse momentum in GeV/c.

The energy resolutions of the electromagnetic and hadron calorimeters are:

$$\frac{\sigma_{E_e}}{E_e} = \frac{10\%}{\sqrt{E_e}} \oplus 0.6\%, \quad \frac{\sigma_{E_h}}{E_h} = \frac{50\%}{\sqrt{E_h}} \oplus 4\%, \quad (2)$$

where E_e and E_h are the energies of electrons and hadrons in GeV. The polar angular coverage of the central tracker maintaining the resolution is $|\cos \theta| < 0.85$, above this range the tracking resolution deteriorates. The electromagnetic and hadron calorimeters cover $|\cos \theta| < 0.996$ maintaining the resolution over the whole angular range. The simulation of the detector is done using the SIMDET [7] package.

The event reconstruction is done in terms of particle flow objects. First, tracks are measured with the tracking system and associated to calorimeter clusters to define charged particle flow objects of electrons, muons and charged hadrons. Since the momentum measurement by the tracking system is much more accurate than the angular and energy measurements with calorimeters, the tracking information is used for the determination of the four-momentum of charged particles. Calorimetric clusters with no associated track are regarded as neutral particle flow objects originating

from photons and neutral hadrons. Measurements of the four-momentum of neutral objects are solely based on the calorimetric information.

3 Physics Processes

At a centre-of-mass energy of $\sqrt{s} = 350$ GeV, the dominant process for light Higgs boson production in the Standard Model is $e^+e^- \rightarrow ZH$. Events of this process, hereafter referred to as signal, are generated using PYTHIA [8] for Higgs boson masses, m_H , of 120 GeV, 150 GeV and 180 GeV. For the Higgs boson, all decay modes are simulated as expected in the Standard Model. The decay modes into hadrons, WW and ZZ are investigated in detail. Z decays are considered into electrons, muons and hadrons. The Standard Model cross sections are given in Table 1 for the investigated signal channels.

decay mode	topology	cross section, fb		
		120 GeV	150 GeV	180 GeV
$ZH \rightarrow \ell^+\ell^-\bar{q}q, ZH \rightarrow \ell^+\ell^-gg$	2 ℓ +2-jets	8.8	2.0	0.06
$ZH \rightarrow q\bar{q}q'\bar{q}', ZH \rightarrow q\bar{q}gg$	4-jets	91.9	20.4	0.62
$ZH \rightarrow \ell^+\ell^-WW, W \rightarrow q\bar{q}'$	2 ℓ +4-jets	0.6	2.6	2.6
$ZH \rightarrow q\bar{q}WW, W \rightarrow q\bar{q}'$	6-jets	6.0	26.5	26.6
$ZH \rightarrow \ell^+\ell^-ZZ, Z \rightarrow q\bar{q}$	2 ℓ +4-jets	0.08	0.33	0.17
$ZH \rightarrow q\bar{q}ZZ, Z \rightarrow q\bar{q}$	6-jets	0.82	3.46	1.73
$ZH \rightarrow$ all final states		160.3	123.7	89.0

Table 1: The cross sections, in fb, times the branching fractions of the investigated signal final states for Higgs boson masses of 120 GeV, 150 GeV and 180 GeV as predicted in the Standard Model for $\sqrt{s} = 350$ GeV. Also given is the total cross section for $e^+e^- \rightarrow ZH$. The cross sections are calculated with PYTHIA taking into account initial state radiation.

For background estimations events are generated with PYTHIA for the processes $e^+e^- \rightarrow q\bar{q}(\gamma)$, $e^+e^- \rightarrow W^+W^-$, $e^+e^- \rightarrow Z(\gamma^*)Z(\gamma^*)$ and $e^+e^- \rightarrow \gamma^*\gamma^*e^+e^- \rightarrow f\bar{f}e^+e^-$. Six fermion final states resulting from the triple gauge boson production are generated with the WHIZARD package [9]. The cross sections of the main background reactions are given in Table 2. The numbers of events generated for each background channel as well as the number of generated signal events correspond to an integrated luminosity of 500 fb^{-1} .

Initial state radiation is simulated by PYTHIA. Beamstrahlung is taken into account using the CIRCE program [10].

background process	cross section, fb	events
$e^+e^- \rightarrow \gamma^*\gamma^*e^+e^- \rightarrow ffe^+e^-$	4.0×10^6	2.0×10^9
$e^+e^- \rightarrow q\bar{q}(\gamma)$	2.7×10^4	1.4×10^7
$e^+e^- \rightarrow W^+W^-$	1.3×10^4	6.5×10^6
$e^+e^- \rightarrow Z(\gamma^*)Z(\gamma^*)$	1.0×10^3	5.0×10^5
$e^+e^- \rightarrow W^+W^-Z$	13.2	6.5×10^3
$e^+e^- \rightarrow ZZZ$	0.48	9.6×10^2

Table 2: The cross sections, in fb, and the numbers of events expected for the important background processes at a centre-of-mass energy 350 GeV. An integrated luminosity of 500 fb^{-1} is assumed.

4 Analysis Procedure

The measurement of the Higgs boson mass is based on the reconstruction of the exclusive final states $ZH \rightarrow \ell^+\ell^-q\bar{q}$, $ZH \rightarrow q\bar{q}q'\bar{q}'$, $ZH \rightarrow \ell^+\ell^-WW$ and $ZH \rightarrow q\bar{q}WW$. In the latter two cases, the contributions from the $ZH \rightarrow \ell^+\ell^-ZZ$ and $ZH \rightarrow q\bar{q}ZZ$ final states are also taken into account.

The analysis in all channels proceeds as follows. First, a selection of events of the specific topology is applied to the samples of signal and background events exploiting event shape variables and lepton identification. For Higgs boson masses below 150 GeV, the decay $H \rightarrow b\bar{b}$ is dominant, leading to $2\ell+2$ -jet and 4-jet topologies. For larger Higgs boson masses, the $H \rightarrow WW$ decay becomes dominant, leading to $2\ell+4$ -jet and 6-jet final states. For their study, jet identification is crucial. A kinematic fit imposing energy and momentum conservation improves considerably the di-jet or 4-jet mass resolutions, and hence the accuracy of the mass measurement. In order to construct the covariance matrix used in the kinematic fit, the resolutions of the lepton and jet energies and angular measurements are needed. For the lepton momentum, the tracker resolution from Equation (1) is used. The resolution in the polar and azimuthal angles, θ and ϕ , of the lepton momentum vector are obtained from Monte Carlo as:

$$\sigma_\theta = 1 \text{ mrad}, \quad \sigma_\phi = \frac{\sigma_\theta}{\sin \theta}. \quad (3)$$

The resolutions of the jet energies and angular measurements are obtained from a Monte Carlo study using the sub-detector resolutions from Equations (1) and (2). They are parameterized as:

$$\sigma_E/E = \frac{30\%}{\sqrt{E}}, \quad \sigma_\theta = 15 \text{ mrad}, \quad \sigma_\phi = \frac{\sigma_\theta}{\sin \theta}, \quad (4)$$

where E is the energy, θ the polar and ϕ the azimuthal angle of the jet.

The Higgs boson mass is obtained by fitting the invariant mass spectrum of the jets assigned to the Higgs boson decay with a superposition of

signal and background distributions. The shape of the signal distribution is derived from a high statistics Monte Carlo sample of signal events and kept fixed in the fit. Free parameters are the peak value and the normalisation factor of the signal distribution.

4.1 The $ZH \rightarrow \ell^+ \ell^- q \bar{q}$ and $ZH \rightarrow q \bar{q} q' \bar{q}'$ Final States

These final states are characterized by two isolated leptons and two jets or by four jets and have the full energy deposited in the detector. Hence, events where the total energy visible in the detector is less than 80% of the centre-of-mass energy are rejected. Global event characteristics are used for the signal selection.

For the channel $ZH \rightarrow \ell^+ \ell^- q \bar{q}$, the number of reconstructed particles must be greater than 20, the event thrust, T , must be less than 0.85 and the absolute value of the cosine of the polar angle of the thrust vector, $\cos \theta_T$, must be less than 0.9. Electrons are identified as energy deposits in the electromagnetic calorimeter whose shape is compatible with the expectation for an electromagnetic shower and with a matched track in the central tracker. The measured track momentum and shower energy must be in agreement within 5% and the shower leakage into the hadron calorimeter must be less than 2 GeV. Muons are tracks pointing to energy deposits in the calorimeters which are consistent with the expectation for a minimum ionizing particle. A pair of electrons or muons with opposite charge is required. Both electrons and muons must have momenta larger than 10 GeV/c and fulfill the polar angle cut $|\cos \theta_\ell| < 0.9$. Leptons must satisfy isolation criteria, meaning that there are no other particles reconstructed within a 15° cone with respect to the lepton momentum vector. The invariant mass of a pair of leptons must be compatible with the mass of the Z boson within 10 GeV. These criteria reduce the backgrounds listed in Table 2 in the selected sample to the level of a few % with the exception of the process $e^+ e^- \rightarrow ZZ$. A cut on the polar angle of the momentum vector of the di-electron or di-muon system, $|\cos \theta_{\ell\ell}| < 0.9$, further suppresses the ZZ background. The signal selection efficiency is about 45%. All reconstructed particles, except the two isolated leptons, are grouped into two jets using the Durham [11] jet clustering algorithm.

Event selection for the $ZH \rightarrow q \bar{q} q' \bar{q}'$ channel is performed by requiring the number of reconstructed particles to be larger than 40, $T < 0.85$ and $|\cos \theta_T| < 0.8$. No isolated leptons with an energy greater than 10 GeV are allowed. Reconstructed particles are grouped into four jets using the Durham jet clustering algorithm. Events are retained if the jet resolution parameter, for which the event is resolved from the four- to three-jet topology, y_{34} , fulfill the relation $\log(y_{34}) > -5$.

The selected events of both final states are subject to a kinematic fit [12] imposing energy and momentum conservation. The kinematic fit is performed by varying the lepton momenta and angles within their resolu-

tions given by Equations (1) and (3), respectively. The jet energies and angles are varied within the corresponding resolutions given by Equations (4).

For events selected as $ZH \rightarrow \ell^+ \ell^- q \bar{q}$, energy and momentum conservation results in four constraints (4C fit). Since the experimental resolution in the invariant mass of the di-lepton system is much smaller than the natural width of the Z boson, no constraint is applied in the kinematic fit to force the di-lepton mass to m_Z . The di-jet invariant mass spectra after the 4C fit are shown in Figure 1 for $m_H = 120$ GeV and 150 GeV, respectively. Clear signals are seen on top of the remaining smooth background from $e^+e^- \rightarrow ZZ$. Also shown are the contributions from $H \rightarrow WW$ and $H \rightarrow ZZ$ decays to the signal. These are negligible for $m_H = 120$ GeV but amount to 62% and 5%, respectively, of the signal for $m_H = 150$ GeV.

The masses obtained from the fits equal the generated Higgs boson masses and have errors of 85 MeV for $m_H = 120$ GeV and 100 MeV for $m_H = 150$ GeV.

For the 4-jet final states, in addition to the four constraints from energy and momentum conservation, the invariant mass of the two jets assigned to the Z boson decay is constrained to m_Z . Hence, a 5C fit is performed for all possible di-jet pairings. The pairing with the minimal χ^2 is chosen. In addition, this χ^2 must be less than 70. The signal selection efficiency is about 25%, however the remaining event sample contains considerable background from $e^+e^- \rightarrow ZZ$, $e^+e^- \rightarrow W^+W^-$ and $e^+e^- \rightarrow q\bar{q}(\gamma)$. The signal-to-background ratio is enhanced using the identification of b-quark jets. The ZVTOP [13] topological vertex finder adapted for the pixel microvertex detector [6] is used to search for secondary vertices inside jets and determine mass, momentum and decay length of the vertex. In addition, the impact parameter joint probability [14] and the two highest impact parameter significances are used as input into neural networks trained with jets containing no, one and more than one secondary vertices. A jet b-tag variable is defined [15] as function of the neural network output x as

$$B(x) = \frac{f_b(x)}{f_b(x) + f_{udsc}(x)},$$

where f_b and f_{udsc} are probability density functions of the neural network outputs in samples of b-jets and udsc-jets, respectively. The improvement in the signal to background ratio can be seen in Figure 2, where invariant mass distributions are shown for the two jets assigned to the Higgs boson decay without a requirement on the jet b-tag variable and for events with at least two jets satisfying $B(x) > 0.2$. The latter requirement keeps the signal statistics almost unchanged but reduces significantly the background. For $m_H = 150$ GeV also events from $ZH \rightarrow q\bar{q}ZZ$ and $ZH \rightarrow q\bar{q}WW$ are selected amounting to 25% of the signal. Using the invariant mass distributions obtained with the requirement $B(x) > 0.2$ the fit of the Higgs

boson mass is performed. As an example, the di-jet invariant mass distribution and the fitted function of the signal is shown in Figure 3.

The results for the Higgs boson masses are equal to the generated masses. The statistical errors are 45 MeV at $m_H = 120$ GeV and 170 MeV at $m_H = 150$ GeV.

4.2 The $ZH \rightarrow \ell^+ \ell^- WW$ and $ZH \rightarrow q\bar{q}WW$ Final States

We consider W-boson decays into two quarks, hence the topologies of these final states are two isolated leptons accompanied by four jets or six jets, respectively. The requirements for electron and muon identification are the same as in the previous section. Although event selection is optimized specifically for the $ZH \rightarrow \ell^+ \ell^- WW$ and $ZH \rightarrow q\bar{q}WW$ final states, contributions from the $ZH \rightarrow \ell^+ \ell^- ZZ$ and $ZH \rightarrow q\bar{q}ZZ$ channels are also taken into account.

Events are selected with an energy deposited in the detector of more than 80% of the centre-of-mass energy and a number of the reconstructed particles larger than 40.

Events of the final state $ZH \rightarrow \ell^+ \ell^- WW$ must contain a pair of isolated electrons or muons with opposite charges. Furthermore, the event thrust and the polar angle of the thrust vector are used to suppress the dominant background from the WW and ZZ final states. The values of the cuts are $T < 0.95$ and $|\cos \theta_T| < 0.95$. Since the two leptons of $ZH \rightarrow \ell^+ \ell^- WW$ originate from the Z decay, their invariant mass is required to be equal within 10 GeV to m_Z . A cut on the polar angle of the di-lepton momentum vector, $|\cos \theta_{\ell\ell}| < 0.9$, further suppresses the ZZ background. Tracks and calorimetric energy deposits not stemming from the leptons are grouped into four jets using the Durham algorithm. The jet resolution parameter y_{34} must satisfy $\log(y_{34}) > -6.0$.

Then a 4C kinematic fit is performed imposing energy and momentum conservation. Only events for which the χ^2 of the 4C fit is less than 50 are retained in the selected sample. The signal selection efficiency amounts to 50% at $m_H = 150$ GeV and 60% at $m_H = 180$ GeV. The 4-jet invariant mass distributions after the kinematic fit are shown in Figure 4 for $m_H = 150$ GeV and 180 GeV.

The fit of the mass spectra in Figure 4 again results in mass values for the Higgs boson equal to the generated ones. The uncertainties of the masses amount to 90 and 80 MeV for $m_H = 150$ GeV and $m_H = 180$ GeV, respectively.

The small background in this channel comes mainly from the semileptonic decays of pair produced Z bosons and triple gauge boson production, ZWW, with a leptonic Z decay. Events of the process $ZH \rightarrow \ell^+ \ell^- ZZ$ constitute 13% and 6% of the signal in the selected sample for $m_H = 150$ and 180 GeV, respectively.

The $ZH \rightarrow q\bar{q}WW$ channel is selected by requiring $T < 0.9$ and $|\cos \theta_T|$

< 0.95 . There must be no isolated leptons with an energy greater than 10 GeV. The reconstructed particles are grouped into six jets using Durham jet algorithm. The jet resolution parameter, for which an event is resolved from the 6- to 5-jet topology, y_{56} , must satisfy $\log(y_{56}) > -8$. Then a likelihood discriminant, L_{HZ} , is defined using as input the number of particles reconstructed in an event, the polar angle of the thrust vector and the jet resolution parameters y_{34} and y_{56} . Events are accepted when the value of this discriminant is larger than 0.9. As an example, Figure 5 shows the distribution of L_{HZ} for the signal events for $m_{\text{H}} = 180$ GeV and the background processes. The six jets are now grouped in three di-jet pairs following criteria which depend on the mass of the Higgs boson. For $m_{\text{H}} < 2m_{\text{W}}$ usually only one W is expected to be on the mass shell, while the other is produced with a mass close to the difference between m_{H} and m_{W} . The quantity

$$\chi^2 = (m_{\text{ij}} - m_{\text{Z}})^2/\sigma_{\text{Z}}^2 + (m_{\text{kl}} - m_{\text{W}})^2/\sigma_{\text{W}}^2 + (m_{\text{mnn}} - m_{\text{klmnn}} + m_{\text{W}})^2/\sigma_{\text{W}^*}^2$$

is calculated for all possible di-jet combinations, where m_{ij} is the invariant mass of the two jets assigned to the Z boson, m_{kl} the invariant mass of two jets assigned to the on-shell W boson, m_{mnn} the invariant mass of two jets assigned to the off-shell W boson and m_{klmnn} the invariant mass of the four jets assigned to decay $\text{H} \rightarrow \text{WW}^*$. The quantities σ_{Z}^2 , σ_{W}^2 and $\sigma_{\text{W}^*}^2$ are obtained from Monte Carlo studies as the convolution of the bosonic widths and the mass resolutions and are estimated to be 6, 9 and 15 GeV, respectively. For $m_{\text{H}} > 2m_{\text{W}}$ both W bosons are on shell. Hence all di-jet combinations are taken and the quantity

$$\chi^2 = (m_{\text{ij}} - m_{\text{Z}})^2/\sigma_{\text{Z}}^2 + (m_{\text{kl}} - m_{\text{W}})^2/\sigma_{\text{W}}^2 + (m_{\text{mnn}} - m_{\text{W}})^2/\sigma_{\text{W}}^2$$

is calculated. The jet pairing with the smallest value of χ^2 is chosen and subject of a kinematic fit imposing energy-momentum conservation and constraining the mass of the two jets assigned to the Z boson to m_{Z} . Events are selected into the final sample if the χ^2 of the 5C fit is less than 30. In addition, the fitted mass of the jets originating from the on-shell W decay must be equal to m_{W} within 20 GeV in the event sample selected for $m_{\text{H}} = 150$ GeV. For $m_{\text{H}} = 180$ GeV, the sum and the difference of the fitted masses of the two jet pairs assigned to a W decay must be between 125 GeV and 185 GeV and -20 and 20 GeV, respectively. The signal selection efficiency amounts to about 20%. The sample selected for $m_{\text{H}} = 150$ GeV also contains 5% signal from the $\text{ZH} \rightarrow \text{q}\bar{\text{q}}\text{q}'\bar{\text{q}}'$ final state.

The distribution of the invariant mass of the 4-jet system is shown in Figure 6 for $m_{\text{H}} = 150$ GeV and 180 GeV, respectively. From the fit approximating the signal by a Gaussian the uncertainties of the masses are 100 MeV and 150 MeV for $m_{\text{H}} = 150$ GeV and 180 GeV, respectively. The background in this channel originates from $e^+e^- \rightarrow \text{W}^+\text{W}^-$, $e^+e^- \rightarrow \text{ZZ}$ and $e^+e^- \rightarrow \text{q}\bar{\text{q}}(\gamma)$ final states, and from triple gauge boson production processes. Events of the process $\text{ZH} \rightarrow \text{q}\bar{\text{q}}\text{ZZ}$ constitute 9% and 5% of the signal in the selected sample for $m_{\text{H}} = 150$ and 180 GeV, respectively.

4.3 Combined Results

Table 3 summarizes the statistical accuracy on the determination of m_H for the different final states and their combination. It should be noted that considerable overlap exists in the selected samples of the $ZH \rightarrow \ell^+\ell^-\text{q}\bar{\text{q}}$ and $ZH \rightarrow \ell^+\ell^-\text{WW}$ channels and of the $ZH \rightarrow \text{q}\bar{\text{q}}\text{q}'\bar{\text{q}}'$ and $ZH \rightarrow \text{q}\bar{\text{q}}\text{WW}$ channels. Hence, the combination is performed only for the non-overlapping topologies which gives a minimal combined error on the Higgs boson mass. This is done using the formula:

$$\frac{1}{\Delta^2(m_H)} = \sum_i \frac{1}{\Delta_i^2(m_H)},$$

where Δ is the combined error, whereas Δ_i is the error obtained in the i^{th} channel.

Decay mode	$\Delta(m_H)$ in MeV		
	120	150	180
$ZH \rightarrow \ell^+\ell^-\text{q}\bar{\text{q}}$	85	100	–
$ZH \rightarrow \text{q}\bar{\text{q}}\text{q}'\bar{\text{q}}'$	45	170	–
$ZH \rightarrow \ell^+\ell^-\text{WW}$	–	90	80
$ZH \rightarrow \text{q}\bar{\text{q}}\text{WW}$	–	100	150
Combined	40	65	70

Table 3: Uncertainties on the determination of the Higgs boson mass for $m_H = 120, 150$ and 180 GeV. The $ZH \rightarrow \ell^+\ell^-\text{WW}$ and $ZH \rightarrow \text{q}\bar{\text{q}}\text{WW}$ channels are used for the combination at $m_H = 150$ GeV.

5 Beam Related Systematic Effects

We have investigated the effect of a bias in the beam energy measurement, of the beam energy spread and of an uncertainty in the differential luminosity spectrum on the measurement of the Higgs boson mass.

The impact of a bias in the beam energy measurement is estimated by generating signal samples with both positron and electron beam energies shifted with respect to the nominal value of $\sqrt{s}/2$. These shifts are varied from -100 MeV to 100 MeV in 25 MeV steps. Since in the kinematical fit the energy is constrained to the nominal value, $\sqrt{s} = 350$ GeV, the shift in the beam energy is expected to result in a shift in the measured Higgs boson mass.

As an example Figure 7 shows the distributions of fitted values of m_H in the $ZH \rightarrow \ell^+\ell^-\text{q}\bar{\text{q}}$ channel for shifts in the beam energies of $+25$ MeV, zero MeV and -25 MeV. In each of the three considered cases the distribution of m_H is obtained from 200 statistically independent signal samples.

The shift obtained in the fit of m_H corresponds roughly to the shift of the beam energy with opposite sign. In the range of beam energy shifts from -100 to 100 MeV the shift in the Higgs boson mass is found to depend linearly on the shift in the beam energy:

$$\delta m_H = -\alpha \cdot \delta E_b, \quad (5)$$

with $\alpha = 0.85$ for the $ZH \rightarrow q\bar{q}q'\bar{q}'$ channel, 0.80 for the $ZH \rightarrow q\bar{q}WW$ channel, and 1.04 for the $ZH \rightarrow \ell^+\ell^-q\bar{q}$ and $ZH \rightarrow \ell^+\ell^-WW$ channels. Hence, in order to keep the systematic bias in m_H well below its statistical error, the beam energy measurement must be controlled with a precision better than 10^{-4} .

To estimate the impact of a beam energy spread, a Gaussian distribution of the beam energy has been used for the generation of signal events. As an example, Figure 8 shows the reconstructed Higgs boson mass spectrum for a sample of $ZH \rightarrow q\bar{q}q'\bar{q}'$ events for a 1% energy spread for both electron and positron beams and the same distribution for a fix beam energy of $\sqrt{s}/2$. The inclusion of this beam energy spread slightly broadens the mass distribution and degrades the precision obtained for m_H from 45 MeV to 50 MeV in the $ZH \rightarrow q\bar{q}q'\bar{q}'$ channel and from 85 MeV to 90 MeV in the $ZH \rightarrow \ell^+\ell^-q\bar{q}$ channel. For the TESLA machine the expected energy spread amounts to 0.15% for the electron beam and 0.03% for the positron beam [6]. For these values of the beam energy spread, no significant degradation of the precision in the Higgs boson mass measurement is observed.

The energy spectra of the colliding electrons and positrons at a high energy linear collider will be significantly affected by photon radiation of the particles in one bunch in the coherent field of the opposite bunch. This effect is referred to as beamstrahlung. The program CIRCE provides a fast simulation of the beamstrahlung under the assumptions that the beamstrahlung in the two beams is equal and uncorrelated between the beams. The spectrum is parameterized according to

$$f(x) = a_0\delta(1-x) + a_1x^{a_2}(1-x)^{a_3},$$

where x is the ratio between the energies of the colliding electron and positron and the initial energy of the undisrupted beam. The parameters a_i depend on the operational conditions of the linear collider. The normalization condition, $\int f(x)dx = 1$, fixes one of these parameters, leaving only three of them independent. The default parameters for the TESLA machine operated at the centre-of-mass energy of 350 GeV are:

$$a_0 = 0.55, \quad a_1 = 0.59, \quad a_2 = 20.3, \quad a_3 = -0.63.$$

It has been shown that from the analysis of the acollinearity spectrum of Bhabha scattering events, the parameters a_i can be determined with a precision of about 1% [16]. To visualize the effect of the uncertainty in the determination of the parameters a_i , the beam energy spectra are shown

in Figure 9 for nominal values of the parameters a_i and for the parameter a_0 shifted by $\pm 10\%$ from its nominal value. Figure 10 presents the corresponding Higgs boson mass spectra at the sample of $ZH \rightarrow \ell^+ \ell^- q \bar{q}$ events. An uncertainty of 10% in the determination of the parameters a_0 results in a systematic uncertainty of about 10 MeV on the Higgs boson mass in the $ZH \rightarrow \ell^+ \ell^- q \bar{q}$ and $ZH \rightarrow q \bar{q} q' \bar{q}'$ channels. The same result is obtained for the other parameters. The uncertainty is reduced to about 1 MeV if the parameters a_i are measured with an accuracy of 1%. The same result is obtained for the study of the $ZH \rightarrow \ell^+ \ell^- WW$ and $ZH \rightarrow q \bar{q} WW$ channels.

6 Conclusion

The potential of the future linear e^+e^- collider for the measurement of the Higgs boson mass is evaluated. Assuming an integrated luminosity of 500 fb^{-1} , the Higgs boson mass can be measured with a statistical accuracy ranging from 40 MeV to 70 MeV for m_H between 120 GeV and 180 GeV. In order to keep the systematic uncertainty due to a bias of the beam energy measurement well below the statistical uncertainty, the beam energy measurement has to be controlled with a precision better than 10^{-4} . Under operational conditions envisaged for the TESLA machine, the beam energy spread and uncertainty in the differential luminosity spectrum are found to have negligible effect on the Higgs boson mass measurement.

7 Acknowledgments

We would like to thank Prof. K. Desch for many helpful discussions and his continuous interest and support.

References

- [1] S.L. Glashow, Nucl. Phys. **22** (1961) 579; S. Weinberg, Phys. Rev. Lett. **19** (1967) 1264; A. Salam, *Elementary Particle Theory*, edited by N. Svartholm (Almqvist and Wiksell, Stockholm, 1968), p. 367.
- [2] P.W. Higgs, Phys. Lett. **12** (1964) 132, Phys. Rev. Lett. **13** (1964) 508 and Phys. Rev. **145** (1966) 1156 ; F. Englert and R. Brout, Phys. Rev. Lett. **13** (1964) 321; G.S. Guralnik, C.R. Hagen and T.W.B. Kibble, Phys. Rev. Lett. **13** (1964) 585.
- [3] ATLAS Collaboration, "ATLAS: Detector and Physics Performance Technical Design Report, Volume 2", CERN-LHCC-99-15, ATLAS-TDR-15 (1999); CMS Collaboration, "CMS Technical Proposal", CERN/LHCC/94-38 (1994).

- [4] P. Garcia-Abia and W. Lohmann, EPJdirect **C2** (2000) 1, A. Juste, hep-ex/9912041.
- [5] N. Meyer and K. Desch, Eur. Phys. J. **C 35** (2004) 171.
- [6] F. Richard, J.R. Schneider, D. Trines and A. Wagner, "TESLA : Technical Design Report", DESY 2001-01, ECFA 2001-209, TESLA Report 2001-023, TESLA-FEL 2001-05 (2001).
- [7] SIMDET V3.2, M. Pohl and H.J. Schreiber, DESY-99-030 (1999).
- [8] PYTHIA V6.136, T. Sjöstrand, Comp. Phys. Comm. **82** (1994) 74.
- [9] W. Kilian, WHIZARD 1.24, LC Note LC-TOOL-2001-039 (2001).
- [10] CIRCE V6, T. Ohl, Comp. Phys. Comm. **94** (1996) 53.
- [11] S. Catani *et al.*, Phys. Lett. **B 269** (1991) 432;
S. Bethke *et al.*, Nucl. Phys. **B 370** (1992) 310.
- [12] V. Blobel, "Constrained Least Squares and Error Propagation", Hamburg (1997).
- [13] T. Kuhl, Nucl. Instr. and Meth. **A 511** (2003) 221;
D. Jackson, Nucl. Instr. and Meth. **A 388** (1997) 247.
- [14] R. Barate *et al.*, Phys. Lett. **B 401** (1997) 150.
- [15] K. Desch *et al.*, LC Note LC-PHSM-2004-006 (2004).
- [16] K.Mönig, LC Note LC-PHSM-2000-060 (200).

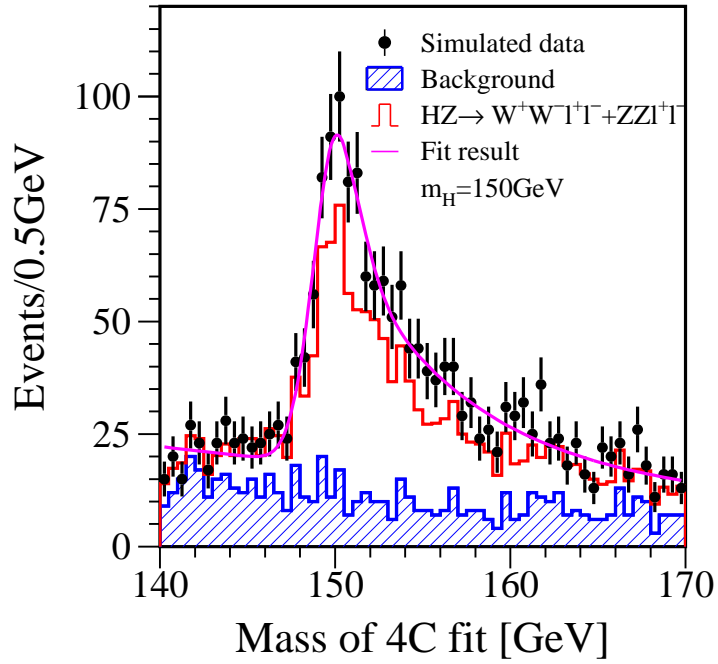
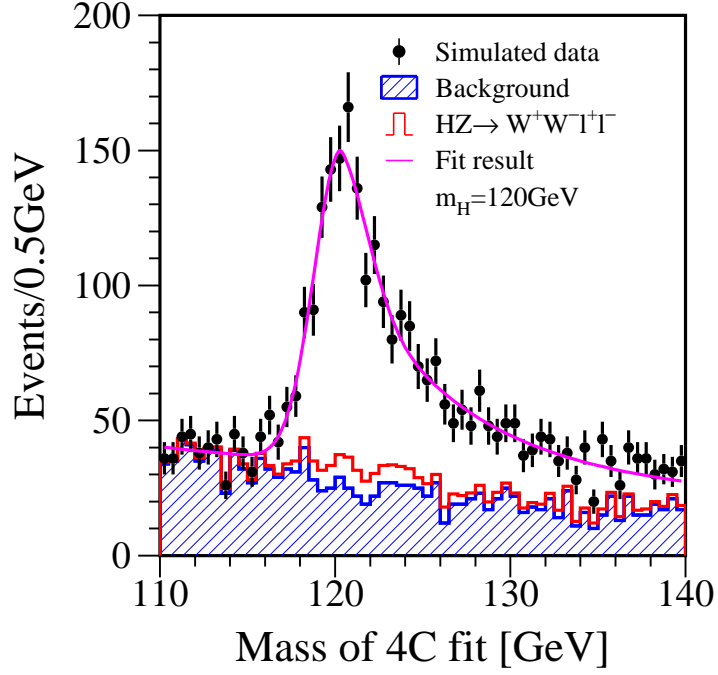


Figure 1: The di-jet invariant mass from the $ZH \rightarrow \ell^+\ell^-\text{q}\bar{\text{q}}$ final state after a 4C kinematic fit for $m_H = 120 \text{ GeV}$ (top) and 150 GeV (bottom).

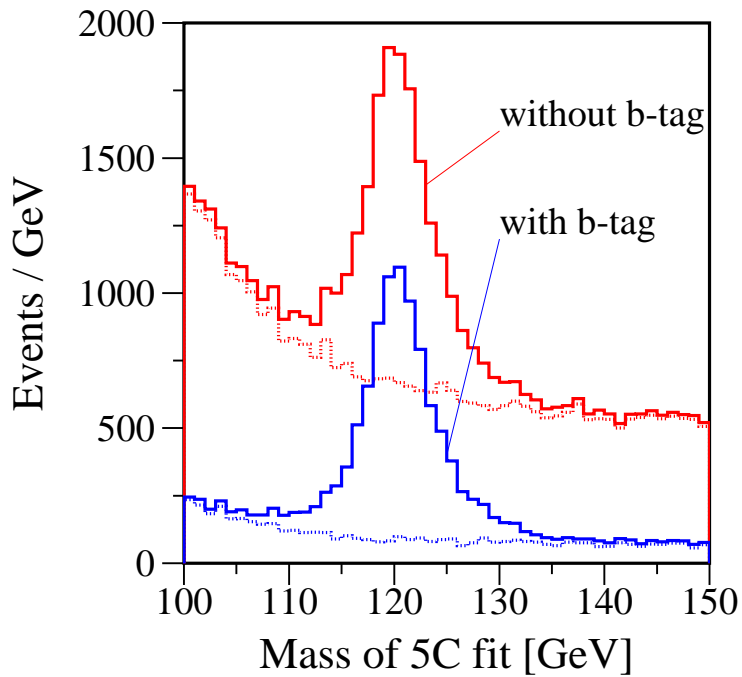


Figure 2: The distribution of the invariant mass of the two jets assigned to the Higgs boson decay in the $ZH \rightarrow q\bar{q}q'\bar{q}'$ final state without requirement on the b-tag and after requiring the values of the b-tag of two jets to be larger than 0.2.

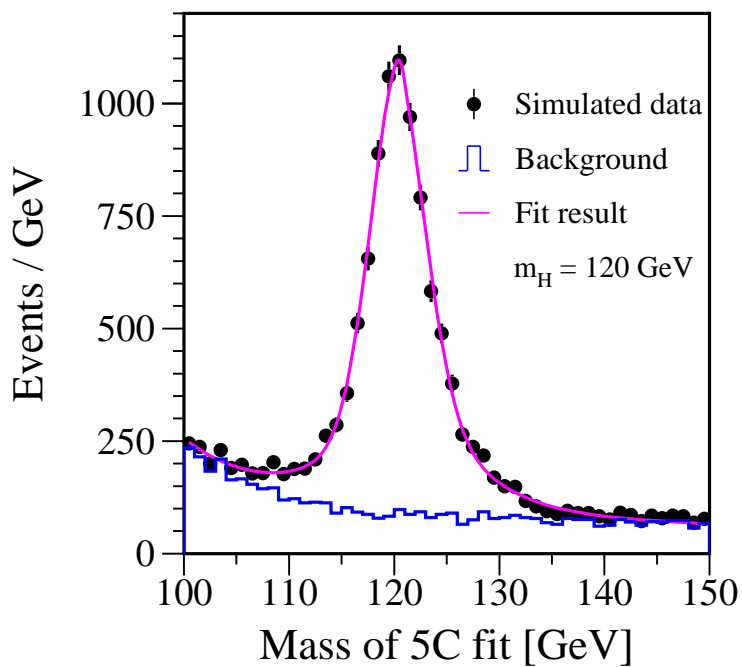


Figure 3: The invariant mass of the two jets assigned to the Higgs boson decay in the $ZH \rightarrow q\bar{q}q'\bar{q}'$ final state after the 5C kinematic fit for $m_H = 120$ GeV. For two jets the b-tag must be larger than 0.2.

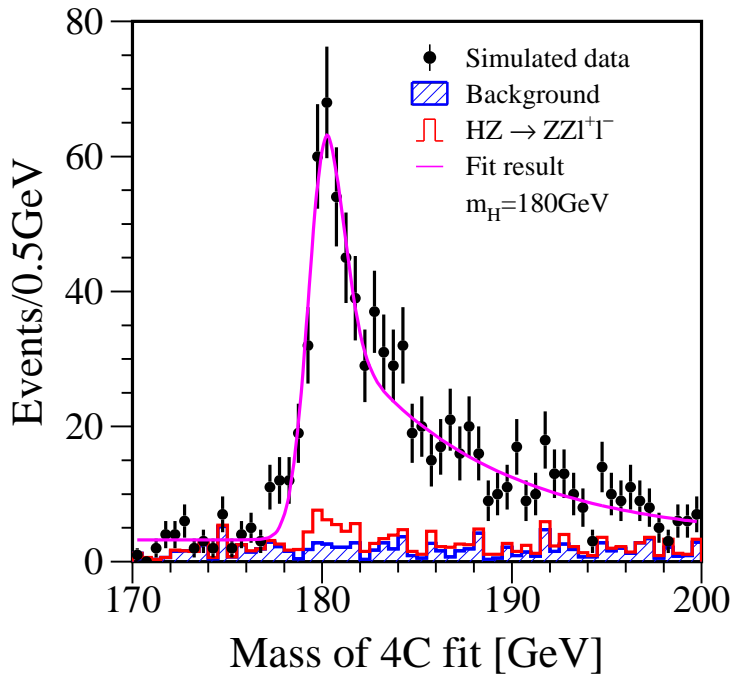
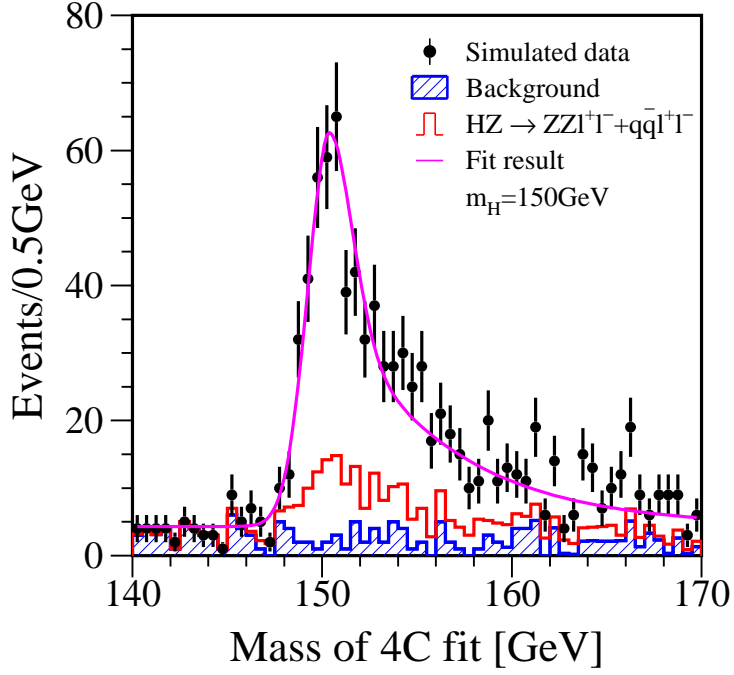


Figure 4: The 4-jet invariant mass from the $ZH \rightarrow \ell^+ \ell^- WW$ final state after a 4C kinematic fit for $m_H = 150 \text{ GeV}$ (top) and 180 GeV (bottom).

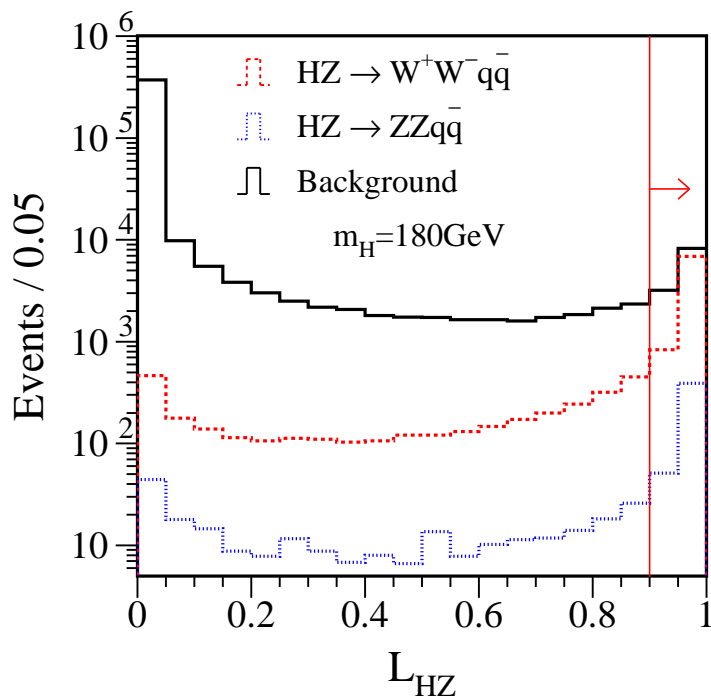


Figure 5: The distributions of the signal likelihood used to select $H \rightarrow WW \rightarrow 6\text{-jet}$ final states for $m_H = 180 \text{ GeV}$. Solid, dashed and dotted lines represent the background processes, $ZH \rightarrow q\bar{q}WW$ and $ZH \rightarrow q\bar{q}ZZ$ signals. The vertical line indicates the cut imposed on this quantity.

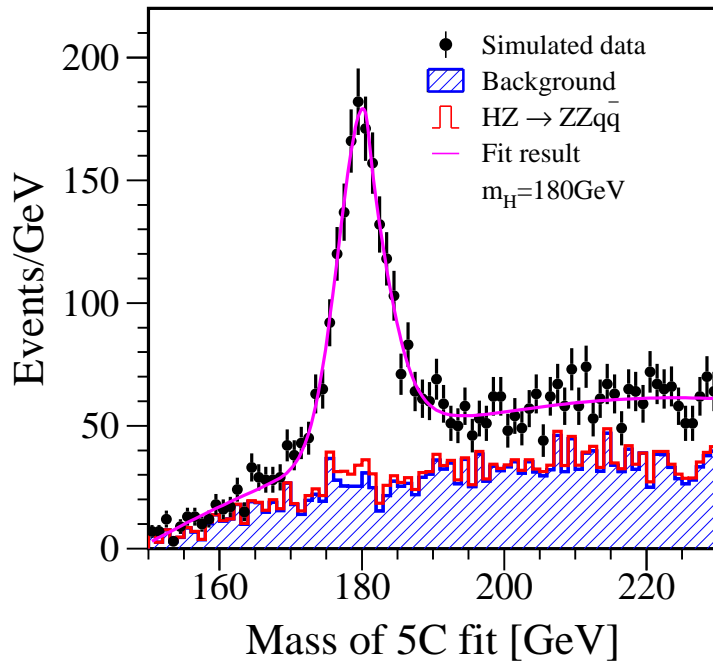
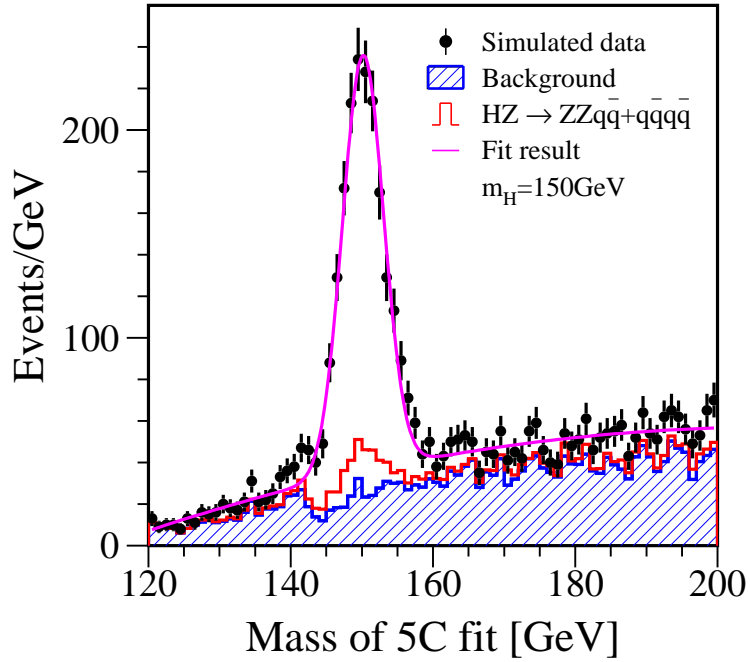


Figure 6: The four jet invariant mass from the $ZH \rightarrow q\bar{q}WW$ final state after a 5C kinematic fit for $m_H = 150 \text{ GeV}$ (top) and $m_H = 180 \text{ GeV}$ (bottom).

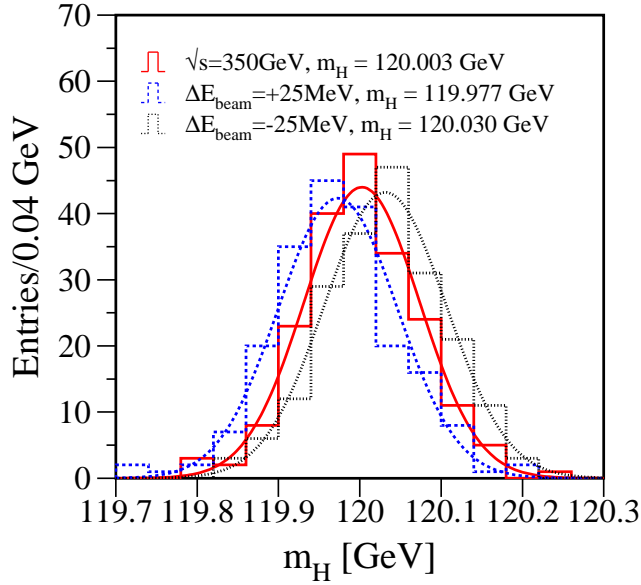


Figure 7: The spectrum of the fitted values of the Higgs boson mass as obtained from 200 independent signal samples for the case when both electron and positron beam energies are overestimated by 25 MeV (dotted histogram), when they are underestimated by 25 MeV (dashed histogram) and when no shifts are introduced to the beam energies (solid histogram).

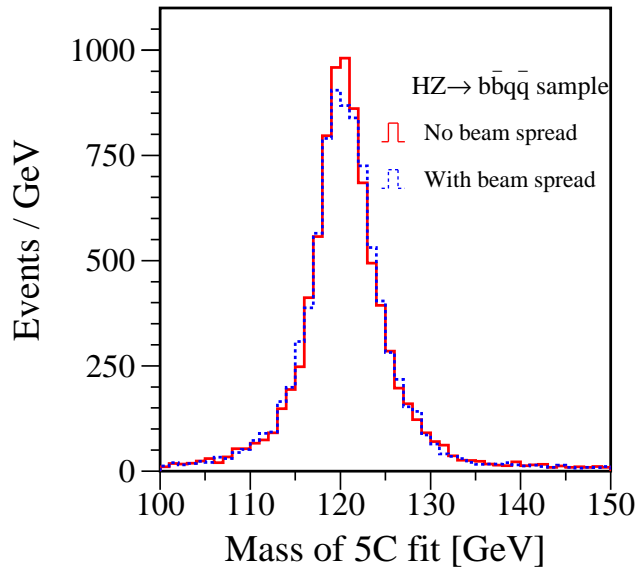


Figure 8: Reconstructed Higgs boson mass spectrum in the sample of the $ZH \rightarrow q\bar{q}q'\bar{q}'$ events for the case of monochromatic beams (solid histogram) and for the case of 1% Gaussian energy spread for both electron and positron beams (dashed histogram).

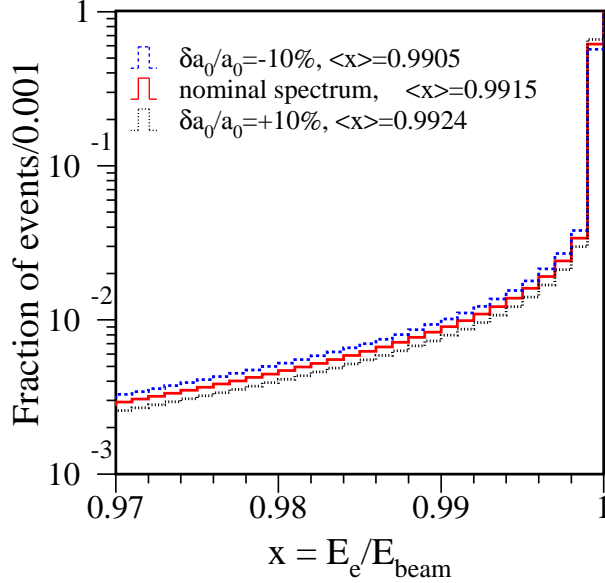


Figure 9: The beam energy spectrum after beamstrahlung for nominal parameters a_i at $\sqrt{s} = 350$ GeV (solid histogram) and for the cases when the parameter a_0 is shifted from its nominal value by -10% (dashed histogram) and +10% (dotted histogram). E_e is the energy of the colliding particle including beamstrahlung and E_{beam} is the nominal beam energy.

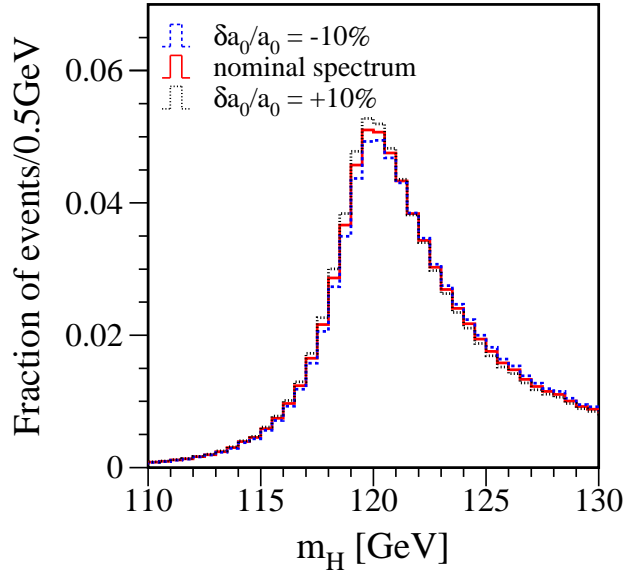


Figure 10: The reconstructed Higgs boson mass spectrum in the sample of $ZH \rightarrow \ell^+ \ell^- q \bar{q}$ events for nominal parameters a_i (see text) at 350 GeV centre-of-mass energy (solid histogram) and for the cases when parameter a_0 is shifted from its nominal value by -10% (dashed histogram) and +10% (dotted histogram).